Theoretical and Applied Fracture Mechanics 51 (2009) 33–40

Contents lists available at ScienceDirect

Theoretical and Applied Fracture Mechanics

journal homepage: www.elsevier.com/locate/tafmec

Multiscale material modeling and its application to a dynamic crack propagation problem

J.D. Lee [a,*], X.Q. Wang [a], Y.P. Chen [b]

[a] Department of Mechanical and Aerospace Engineering, The George Washington University, Washington, DC 20052, United States
[b] Department of Mechanical and Aerospace Engineering, University of Florida, Gainesville, Florida 32611, United States

ARTICLE INFO

Article history:
Available online 23 January 2009

Keywords:
Multiscale modeling
Multi-grain material system
Crack propagation
Single crystal
Grain boundary
Finite element
Molecular dynamics

ABSTRACT

Here we present a multiscale field theory for modeling and simulation of multi-grain material system which consists of several different kinds of single crystals and a large number of different kinds of discrete atoms. The theoretical construction of the multiscale field theory is briefly introduced. The interatomic forces are used to formulate the governing equations for the system. A compact tension specimen made of magnesium oxide is modeled by discrete atoms in front of the crack tip and finite elements in the far field. Results showing crack propagation through the atomic region are presented.

1. Introduction

The term 'multiscale material modeling' refers to theory and simulation of material properties and behavior across length and time scales from the atomistic to the macroscopic. With the increase in the application of new experimental tools and new material synthesis techniques to nano/micro systems, multiscale material modeling has emerged as a significant approach in computational materials research. Despite widespread interest and efforts, major challenges exist for the simulation of nano/micro scale systems over a realistic range of time, length, temperature as well as in multiple physical conditions and environments. In the last decade, many concurrent multiscale techniques have been developed. Some of these works will be mentioned and more details can be found in [1,2].

The Quasicontinuum (QC) method was introduced in [3]. It has been further developed and used to study a variety of fundamental aspects of deformation in crystalline solids [4–6]. It is as accurate as molecular dynamics (MD) simulations, but much faster; and it is suitable for large-scale static problems. Using a combination of statistical mechanics and finite element interpolation, the work in [7] developed a coarse-grained alternative to molecular dynamics for crystalline solids at constant temperature.

The Handshaking method [8–11] is a pioneering work, which incorporates tight-binding quantum mechanics approximation, MD, and finite element (FE) continuum model. In this method there is a "hand-shake" domain where the MD model and the continuum model coexist with averaged Hamiltonian. All of the atoms in the "hand-shake" domain are in direct correspondence with nodes of the FE mesh. In the continuum region, all of the FEs are modeled as linearly elastic and the elastic moduli are chosen to exactly match those of the underlying atomistic model, thus minimizing the mismatch across the interface.

A heterogeneous multiscale method [12–14] has been developed by E and his co-workers. It is based on the concept that both the atomistic and the continuum models are formulated in the form of conservation laws of mass, momentum and energy. The strategy is to start with a macroscale solver and find the missing macroscale data such as the constitutive laws and kinetic relation by performing local simulations of the microscale models constrained to be consistent with a local macroscale state of the system.

The Bridging-domain method makes use of the continuum and molecular domains which are overlapped in a bridging subdomain, where the Hamiltonian is taken to be linear combination of the continuum and molecular Hamiltonian [15,16]. The compatibility in the bridging domain is enforced by Lagrange multipliers or by the augmented Lagrangian method. This method is aimed at crystalline or amorphous solids. Results show that this method can avoid spurious wave reflections at the molecular/continuum interface without any additional filtering procedures.

The bridging-scale method concerns with the molecular displacements that are decomposed into fine and coarse scales throughout the domain [17]. At the interface between the two domains, they use a form of the Langevin equation to eliminate

* Corresponding author.
E-mail address: jdlee@gwu.edu (J.D. Lee).

0167-8442/$ - see front matter © 2009 Elsevier Ltd. All rights reserved.
doi:10.1016/j.tafmec.2009.01.003

spurious reflections at the interface. Karpov et al. have developed coupling methods based on lattice dynamics [18]. In this method, the spurious reflections at the edge of the molecular model are eliminated by introducing forces equivalent to the lattice impedance. Proposed in [19] is to combine the bridging-scale method with the perfectly-matched-layer method to eliminate the spurious reflections by matching the impedance at the atomistic/continuum interface.

Generally speaking, in all those above-mentioned coupled methods, the idea is to use a fully atomistic description in one region of material and a continuum description in other regions. The detailed treatment of the material in the 'transition region' or boundary between the atomistic and continuum regions is a critical aspect of such an approach. These methods are reviewed [20] and noted that a unified and formal theory of the transition region that allows quantifiable error bounds to be established.

In a series of theoretical papers, a multiscale field theory [21–27] has been constructed for concurrent atomic–continuum modeling of materials/systems. Continuous local densities of fundamental physical quantities in atomistic systems are derived. Field description of conservation laws at atomic scale has been formulated. As a result of the formulation, a field representation of atomic many-body dynamics is obtained. Since the conservation equations are valid at atomic scale, the field theory can reproduce time-interval averaged atomic trajectories and can be used to investigate phenomena and properties that originated at atomic scale. Since it is a field theory formulated in terms of time-interval averaged quantities, it is expected to be computationally more efficient than atomic-level MD simulation, and can be applied to simulate phenomena at larger length and time scales.

2. Multiscale field theory

Crystalline solids are distinguished from other states of matter by a periodic arrangement of the atoms; such a structure is called a Bravais lattice. Essentially the regularity displayed by a crystal lattice is that of a three-dimensional mesh which divides space into identical parallelepipeds. Imagine that a number of identical atoms, referred to as a unit cell, are placed at the intersections of such a mesh; then we have a grain or a single crystal. A number of different and distinct grains with grain boundaries in between make a multi-grain material system. In this work, we consider the grain boundaries are in their amorphous phase and modeled as a number of different and distinct atoms. The distinct feature of this multiscale theory is that a single crystal is modeled as a continuum in which a point represents a unit cell consisting of a specified number of distinct and different atoms, not just an idealized mathematical identity. Therefore a multi-grain material system is considered as a concurrent atomic/continuum material system. All single crystals (grains) are modeled by the multiscale theory, a continuum theory, but not just a classical continuum theory in which a point only has three degrees of freedom.

The key points of this multiscale theory [21–29] are briefly introduced here. Microscopic dynamic quantities are functions of phase-space coordinates $(\mathbf{r}, \mathbf{p})$, i.e., the positions and momenta of atoms. Each single crystal is treated as a multi-element system; there is more than one atom in the unit cell. There results

$$\begin{aligned}\mathbf{r} &= \{\mathbf{R}^{k\alpha} = \mathbf{R}^k + \Delta\mathbf{r}^{k\alpha} |\ k = 1,2,3,\ldots n, \quad \alpha = 1,2,3,\ldots v\}\\ \mathbf{p} &= \{m^\alpha \mathbf{V}^{k\alpha} = m^\alpha \mathbf{V}^k + m^\alpha \Delta v^{k\alpha} |\\ &\quad k = 1,2,3\ldots n, \quad \alpha = 1,2,3,\ldots v\}\end{aligned} \tag{1}$$

where the superscript $k\alpha$ refers to the αth atom in the kth unit cell; m^α is the mass of the αth atom; $\mathbf{R}^{k\alpha}$ and $\mathbf{V}^{k\alpha}$ are the position and velocity vector of the $k\alpha$ atom, respectively; $\mathbf{R}^k$ and $\mathbf{V}^k$ are the position and velocity of the mass center of the *kth* unit cell, respectively; $\Delta\mathbf{r}^{k\alpha}$ and $\Delta\mathbf{v}^{k\alpha}$ are the atomic position and velocity of the *αth* atom relative to the mass center of the *kth* unit cell, respectively; n is the total number of unit cells in the system; υ is the number of atoms in a unit cell. The local density of any measurable phase-space function $\mathbf{a}(\mathbf{r}, \mathbf{p})$ can generally be defined as

$$\mathbf{A}(\mathbf{x}, \mathbf{y}^\alpha, t) = \sum_{k=1}^{n} \sum_{\xi=1}^{v} \mathbf{a}\{\mathbf{r}(t), \mathbf{p}(t)\}\delta(\mathbf{R}^k - \mathbf{x})\tilde{\delta}(\Delta\mathbf{r}^{k\xi} - \mathbf{y}^\alpha) \equiv \mathbf{A}^\alpha(\mathbf{x}, t) \tag{2}$$

For example, the mass density and linear momentum density can be defined as

$$\rho^\alpha \equiv \sum_{k=1}^{n} \sum_{\xi=1}^{\upsilon} m^\alpha \delta(\mathbf{R}^k - \mathbf{x})\tilde{\delta}(\Delta\mathbf{r}^{k\xi} - \mathbf{y}^\alpha) \tag{3}$$

$$\rho^\alpha(\mathbf{v} + \Delta\mathbf{v}^\alpha) \equiv \sum_{k=1}^{n} \sum_{\xi=1}^{\upsilon} m^\alpha(\mathbf{V}^k + \Delta\mathbf{v}^{k\alpha})\delta(\mathbf{R}^k - \mathbf{x})\tilde{\delta}(\Delta\mathbf{r}^{k\xi} - \mathbf{y}^\alpha) \tag{4}$$

The first delta function in Eq. (2) is a localization function that provides the link between phase space and physical space descriptions. It can be a Dirac δ-function used in [30], or a distribution function used in [31]

$$\delta(\mathbf{R}^k - \mathbf{x}) = \pi^{-3/2} l^{-3} e^{-|\mathbf{R}^k - \mathbf{x}|/l^2} \tag{5}$$

The second delta function in Eq. (2) is the Kronecker delta, which identifies $\mathbf{y}^\alpha$ to $\Delta\mathbf{r}^{k\alpha}$. It can be easily proved that the following conditions hold

$$\begin{aligned}&\int_{\Omega(\mathbf{x})} \delta(\mathbf{R}^k - \mathbf{x})\tilde{\delta}(\Delta\mathbf{r}^{k\alpha} - \mathbf{y}^\alpha) d^3\Omega(\mathbf{x}) = 1\\ &(k = 1,2,3,\ldots n) \quad (\alpha = 1,2,\ldots v)\end{aligned} \tag{6}$$

$$\frac{\partial\delta(\mathbf{R}^k - \mathbf{x})}{\partial\mathbf{R}^k} = -\frac{\partial\delta(\mathbf{R}^k - \mathbf{x})}{\partial\mathbf{x}}, \frac{\partial\delta(\Delta\mathbf{r}^{k\alpha} - \mathbf{y}^\alpha)}{\partial\Delta\mathbf{r}^{k\alpha}} = -\frac{\partial\delta(\Delta\mathbf{r}^{k\alpha} - \mathbf{y}^\alpha)}{\partial\mathbf{y}^\alpha} \tag{7}$$

The derivative of $\mathbf{A}^\alpha(\mathbf{x}, t)$ with respect to time can be obtained as [22,24]

$$\begin{aligned}\left.\frac{\partial\mathbf{A}^\alpha}{\partial t}\right|_{\mathbf{x},\mathbf{y}^\alpha} &= \sum_{k=1}^{n} \left\{(\mathbf{V}^{k\alpha} \cdot \nabla_{\mathbf{R}^{k\alpha}} + \frac{\mathbf{F}^{k\alpha}}{m^\alpha} \cdot \nabla_{\mathbf{V}^{k\alpha}})\mathbf{a}\right\}\delta(\mathbf{R}^k - \mathbf{x})\tilde{\delta}(\Delta\mathbf{r}^{k\alpha}\\ &\quad - \mathbf{y}^\alpha) - \nabla_{\mathbf{x}} \cdot \left\{\sum_{k=1}^{n} \mathbf{V}^k \otimes \mathbf{a}\delta(\mathbf{R}^k - \mathbf{x})\tilde{\delta}(\Delta\mathbf{r}^{k\alpha} - \mathbf{y}^\alpha)\right\}\\ &\quad - \nabla_{\mathbf{y}^\alpha} \cdot \left\{\sum_{k=1}^{n} \Delta\mathbf{v}^{k\alpha} \otimes \mathbf{a}\delta(\mathbf{R}^k - \mathbf{x})\tilde{\delta}(\Delta\mathbf{r}^{k\alpha} - \mathbf{y}^\alpha)\right\}\end{aligned} \tag{8}$$

When $\mathbf{A}^\alpha(\mathbf{x}, t)$ a conserved property, Eq. (8) yields a local conservation law that governs the time evolution of $\mathbf{A}^\alpha$.

Most current MD applications involve systems those are either in equilibrium or in some time-independent stationary state; where individual results are subjected to fluctuation; it is the well-defined averages over sufficiently long time intervals that are of interest. To smooth out the results and to obtain results close to experiments, measurements of physical quantities are necessary to be collected and averaged over finite time duration. Therefore, in deriving the field description of atomic quantities and balance equations, it is the time-interval averaged quantities that are used, and the time-interval averaged (at time t in the interval $[t_1 \equiv t - \tilde{t}/2, t_2 \equiv t + \tilde{t}/2]$) local density function takes the form

$$\bar{A}^\alpha(\mathbf{x}, t) \equiv \langle A^\alpha \rangle \equiv \frac{1}{\tilde{t}} \int_{t_1}^{t_2} A^\alpha(\mathbf{x}, \tau) d\tau \tag{9}$$

The mathematical representation of conservation equations for mass, linear momentum and energy at atomic scale in terms of averaged field quantities can be analytically obtained as illustrated

in Eq. (8). Concerned with is the 'one-way coupling' with temperature and electromagnetic fields, i.e., the temperature and electromagnetic fields are given as functions of space and time. Then the relevant governing equations are just the balance laws for linear momentum

$$\frac{\partial}{\partial t}[\bar{\rho}^{\alpha}(\bar{\mathbf{v}}+\Delta\bar{\mathbf{v}}^{\alpha})] = \nabla_{\mathbf{x}}\cdot[\bar{\mathbf{t}}^{\alpha}-\bar{\rho}^{\alpha}\bar{\mathbf{v}}\otimes(\bar{\mathbf{v}}+\Delta\bar{\mathbf{v}}^{\alpha})]+\nabla_{\mathbf{y}^{\alpha}}\cdot[\bar{\tau}^{\alpha}-\bar{\rho}^{\alpha}\Delta\bar{\mathbf{v}}^{\alpha}\otimes(\bar{\mathbf{v}}+\Delta\bar{\mathbf{v}}^{\alpha})]+\langle\boldsymbol{\varphi}^{\alpha}/V\rangle \tag{10}$$

where $\bar{\mathbf{t}}^{\alpha}=\bar{\mathbf{t}}^{\alpha}_{(\mathrm{kin})}+\bar{\mathbf{t}}^{\alpha}_{(\mathrm{pot})}$, $\bar{\tau}^{\alpha}=\bar{\tau}^{\alpha}_{(\mathrm{kin})}+\bar{\tau}^{\alpha}_{(\mathrm{pot})}$ are the time-interval averaged homogeneous and inhomogeneous atomic stresses, respectively; V is the volume of the unit cell; $\langle\bar{\boldsymbol{\varphi}}^{\alpha}/V\rangle$ is the body force density. It is emphasized that the potential parts of the atomic stresses satisfy the following condition

$$\nabla_{\mathbf{x}}\cdot\bar{\mathbf{t}}^{\alpha}_{(\mathrm{pot})}+\nabla_{\mathbf{y}^{\alpha}}\cdot\bar{\tau}^{\alpha}_{(\mathrm{pot})}=\langle\mathbf{f}^{\alpha}/V\rangle \tag{11}$$

where $\mathbf{f}^{\alpha}$ is the interatomic force acting on the αth atom in the unit cell located at $\mathbf{x}$. The kinetic parts of the atomic stresses are obtained as

$$\begin{aligned}\bar{\mathbf{t}}^{\alpha}_{(\mathrm{kin})} &\equiv -\left\langle\sum_{k=1}^{n} m^{\alpha}\tilde{\mathbf{V}}^{k}\otimes\tilde{\mathbf{V}}^{k\alpha}\delta(\mathbf{R}^{k}-\mathbf{x})\tilde{\delta}(\Delta\mathbf{r}^{k\alpha}-\mathbf{y}^{\alpha})\right\rangle,\\ \bar{\tau}^{\alpha}_{(\mathrm{kin})} &\equiv -\left\langle\sum_{k=1}^{n} m^{\alpha}\Delta\tilde{\mathbf{v}}^{k\alpha}\otimes\tilde{\mathbf{V}}^{k\alpha}\delta(\mathbf{R}^{k}-\mathbf{x})\tilde{\delta}(\Delta\mathbf{r}^{k\alpha}-\mathbf{y}^{\alpha})\right\rangle\end{aligned} \tag{12}$$

where

$$\tilde{\mathbf{V}}^{k\alpha}\equiv\mathbf{V}^{k\alpha}-\bar{\mathbf{v}}-\Delta\bar{\mathbf{v}}^{\alpha},\quad \tilde{\mathbf{V}}^{k}\equiv\mathbf{V}^{k}-\bar{\mathbf{v}},\quad \Delta\tilde{\mathbf{v}}^{k\alpha}\equiv\Delta\mathbf{v}^{k\alpha}-\Delta\bar{\mathbf{v}}^{\alpha} \tag{13}$$

The governing equation, (9), can now be rewritten as

$$\bar{\rho}^{\alpha}\ddot{\bar{\mathbf{u}}}^{\alpha}=\nabla_{\mathbf{x}}\cdot\bar{\mathbf{t}}^{\alpha}_{(\mathrm{kin})}+\nabla_{\mathbf{y}^{\alpha}}\cdot\bar{\tau}^{\alpha}_{(\mathrm{kin})}+\langle\mathbf{f}^{\alpha}/V\rangle+\langle\boldsymbol{\varphi}^{\alpha}/V\rangle \tag{14}$$

where $\bar{\mathbf{u}}^{\alpha}$ is the time-interval averaged displacement of the αth atom. For a single-element atomic system, the definitions for kinetic stresses $\hat{t}_{\mathrm{ij}}$ and temperature $\hat{T}$ were given in [32,33]

$$\hat{t}_{\mathrm{ij}}=-\left\langle\sum_{l=1}^{N} m\tilde{\mathbf{v}}^{l}_{i}\tilde{\mathbf{v}}^{l}_{j}\right\rangle\Big/\hat{V},\quad 3Nk_{\mathrm{B}}\hat{T}=\left\langle\sum_{l=1}^{N} m\tilde{\mathbf{v}}^{l}_{i}\tilde{\mathbf{v}}^{l}_{i}\right\rangle \tag{15}$$

where k_{B} is the Boltzmann constant; $\hat{V}$ is the volume that the N atoms occupy. In consistent with the work in [32,33], for multi-element atomic system, we have

$$\begin{aligned}&\bar{\mathbf{t}}^{\alpha}_{(\mathrm{kin})}=-\langle m^{\alpha}\tilde{\mathbf{v}}\otimes(\tilde{\mathbf{v}}+\Delta\tilde{\mathbf{v}}^{\alpha})\rangle/V,\quad \bar{\tau}^{\alpha}_{(kin)}=-\langle m^{\alpha}\Delta\tilde{\mathbf{v}}^{\alpha}\otimes(\tilde{\mathbf{v}}+\Delta\tilde{\mathbf{v}}^{\alpha})\rangle/V,\\ &3k_{\mathrm{B}}T^{\alpha}=\langle m^{\alpha}(\tilde{\mathbf{v}}+\Delta\tilde{\mathbf{v}}^{\alpha})\cdot(\tilde{\mathbf{v}}+\Delta\tilde{\mathbf{v}}^{\alpha})\rangle\end{aligned} \tag{16}$$

It is seen that

$$\bar{\mathbf{t}}^{\alpha}_{(\mathrm{kin})}+\bar{\tau}^{\alpha}_{(\mathrm{kin})}=-\langle m^{\alpha}(\tilde{\mathbf{v}}+\Delta\tilde{\mathbf{v}}^{\alpha})\otimes(\tilde{\mathbf{v}}+\Delta\tilde{\mathbf{v}}^{\alpha})\rangle/V$$

is symmetric; but neither $\bar{\mathbf{t}}^{\alpha}_{(\mathrm{kin})}$ nor $\bar{\tau}^{\alpha}_{(\mathrm{kin})}$ is symmetric. At temperature higher than Debye temperature and within harmonic approximation, all modes have the same energy [34]. This implies

$$(\upsilon-1)\langle M\tilde{\mathbf{v}}\cdot\tilde{\mathbf{v}}\rangle=\left\langle\sum_{\alpha=1}^{\upsilon} m^{\alpha}\Delta\tilde{\mathbf{v}}^{\alpha}\cdot\Delta\tilde{\mathbf{v}}^{\alpha}\right\rangle \tag{17}$$

where $M\equiv\sum_{\alpha=1}^{\upsilon}m^{\alpha}$ is the total mass of a unit cell. Eq. (17) implies

$$\bar{t}^{\alpha}_{(\mathrm{kin})\mathrm{ij}}=-\lambda^{\alpha}k_{\mathrm{B}}T\delta_{\mathrm{ij}}/V,\quad \bar{\tau}^{\alpha}_{(\mathrm{kin})\mathrm{ij}}=-(1-\lambda^{\alpha})k_{B}T\delta_{\mathrm{ij}}/V \tag{18}$$

where $\lambda^{\alpha}\equiv m^{\alpha}/M$. Definition of temperature at nanoscale is still a debating issue. Here, we follow the classical way to define temperature as a measure of thermal energy over a finite duration and over a unit cell. Thus, we have $T^{\alpha}=T(\mathbf{x},t)$ and $\nabla_{\mathbf{y}^{\alpha}}\cdot\bar{\tau}^{\alpha}_{(\mathrm{kin})}=0$. Now the governing equation, Eq. (14), can be rewritten as

$$m^{\alpha}\ddot{\bar{\mathbf{u}}}^{\alpha}(\mathbf{x},t)=-\lambda^{\alpha}k_{\mathrm{B}}\nabla T(\mathbf{x},t)+\bar{\mathbf{f}}^{\alpha}(\mathbf{x},t)+\bar{\boldsymbol{\varphi}}^{\alpha}(\mathbf{x},t) \tag{19}$$

On the other hand, in MD simulation, the governing equation for any individual atom can be written as

$$m^{i}\ddot{\mathbf{u}}^{i}(t)=\mathbf{f}^{i}(t)+\boldsymbol{\varphi}^{i}(t) \tag{20}$$

where m^{i} is the mass of the ith atom, a constant; $\mathbf{u}^{i}(t),\mathbf{f}^{i}(t),\boldsymbol{\varphi}^{i}(t)$ are the displacement of the ith atom, all the interatomic force and the body force acting on the ith atom, respectively. It is emphasized that Eq. (19) is the governing equation for the displacement field, $\bar{\mathbf{u}}^{\alpha}(\mathbf{x},t)$ [α = 1,2,3,...,υ], while Eq. (20) is the governing equations (ordinary differential equations in time) for $\mathbf{u}^{i}(t)$ [i = 1, 2, 3,...,N_{a}], where N_{a} is the number of all atoms in the material system. It is also noticed that temperature is not an independent variable in MD simulation; therefore it doesn't appear in the governing equations; instead it is calculated as

$$3Nk_{\mathrm{B}}T=\left\langle\sum_{i=1}^{N} m^{i}\tilde{\mathbf{v}}^{i}\cdot\tilde{\mathbf{v}}^{i}\right\rangle=\left\langle\sum_{i=1}^{N} m^{i}(\dot{\mathbf{u}}^{i}-\dot{\bar{\mathbf{u}}}^{i})\cdot(\dot{\mathbf{u}}^{i}-\dot{\bar{\mathbf{u}}}^{i})\right\rangle \tag{21}$$

Of course, in calculating the temperature, both the time interval $\tilde{t}$ and the number of atoms N have to be large enough to ensure the statistical meaning.

3. Finite element formulation

Consider the case of zero absolute temperature, i.e., $T=0^{\circ}$K. Practically speaking this approximation means either we consider a low temperature scenario or we neglect the thermal-mechanical coupling. However, mathematically it implies $\dot{\bar{\mathbf{u}}}^{i}=\dot{\mathbf{u}}^{i}$ and hence there is no need to distinguish the instantaneous value of a variable from its time-interval averaged value. Therefore, from now on, if there is no ambiguity, we drop the bar on top of every time-interval averaged quantity.

Consider that the specimen is a multi-grain material system made of two regions, continuum region and atomic region, as shown in Fig. 1. In the continuum region, there are several different kinds of single crystals (grains). Each single crystal is divided into identical parallelepipeds – unit cells. Each unit cell is made of a specified number of distinct atoms. Irregular FE meshes are used, in which each node is a unit cell. To emphasize it graphically, the atoms in the nodes are shown in color; different color represents different kind of atoms. In the atomic region, there are many different and distinct atoms as indicated by different colors. The continuum region and the atomic region are used to model the material in its crystalline phase and amorphous phase, respectively. It is noticed that this material system is more general than a polycrystalline material system, in which all single crystals are same in material but different in size and orientations; also more general than nanoscale devices, which are usually constructed as a layered structure without discrete atoms between layers. In Fig. 2, we see three circles around one atom and two nodes of different grains. The shaded area indicates a *Cutoff* region within which all the atomistic interactions have to be counted. It is seen that the atoms in one grain may have atomistic interaction with atoms in another grains as well as in the atomic region.

In the continuum region, there are N_{g} non-overlapping distinct single crystals; each may be referred to as a grain. The atomic region is employed to model the grain boundary, which is considered as in its amorphous phase. In the atomic region, there are N_{a} discrete atoms. For the *Kth* single crystal (grain), each unit cell has $\upsilon(K)$ atoms; the type of atom is denoted by $\gamma(\alpha,K)$[α = 1,2,3,...,$\upsilon(K)$, K = 1,2,3,...,N_{g}]. For the grain boundary (in amorphous phase), there are N_{a} atoms; the type of atom is denoted by $\gamma(i)$[i = 1,2,3,...,N_{a}].The governing equations in these two regions may be expressed as:

Continuum region [α = 1,2,3,...,$\upsilon(K)$, K = 1,2,3,...,N_{g}]

$$m^{\gamma(\alpha,K)}\ddot{\mathbf{u}}^{\alpha}(\mathbf{x},t)=\mathbf{f}^{\alpha}(\mathbf{x},t)+\boldsymbol{\varphi}^{\alpha}(\mathbf{x},t) \tag{22}$$

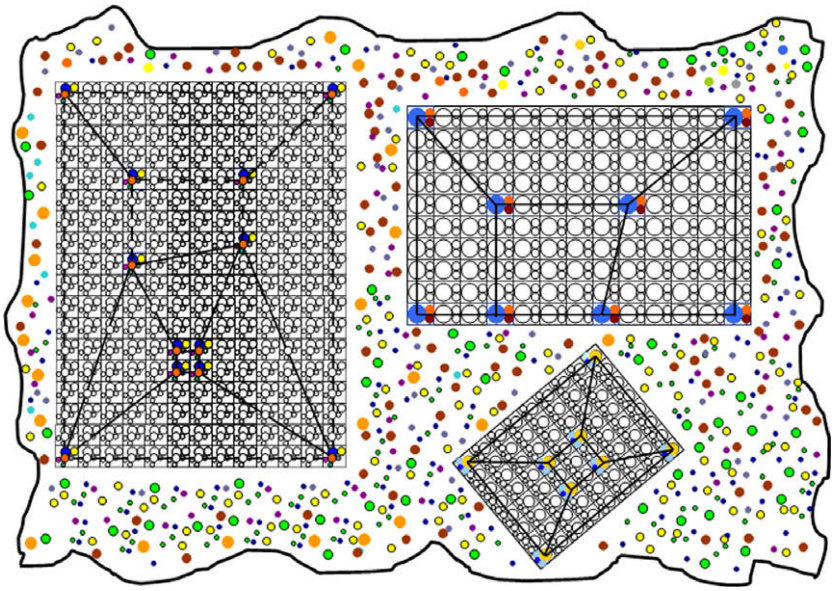

Fig. 1. Schematic diagram of multi-grain material system including crystal lattices, finite element meshes and nodes, and randomly distributed distinct atoms.

where m^{γ} is the mass of the γ-*type* atom; the displacement $\mathbf{u}^{\alpha}(\mathbf{x}, t)$, atomic force $\mathbf{f}^{\alpha}(\mathbf{x}, t)$, and body force due to external field $\boldsymbol{\varphi}^{\alpha}(\mathbf{x}, t)$ are all field variables. The superscript α indicates that for each point in space-time there are $\upsilon(K)$ atoms and hence there are $3\upsilon(K)$ degrees of freedom.

Atomic region $[i = 1,2,3,\ldots,N_a]$

$$m^{\gamma(i)}\ddot{\mathbf{u}}^{i}(t) = \mathbf{f}^{i}(t) + \boldsymbol{\varphi}^{i}(t) \tag{23}$$

where $\gamma(i)$ refers to the type of the *ith* atom whose mass is denoted by $m^{\gamma(i)}$. Opposite to their counter parts in the continuum region, $\mathbf{u}^{i}(t)$, $\mathbf{f}^{i}(t)$, and $\boldsymbol{\varphi}^{i}(t)$ are discrete variables.

Define $\mathbf{f}^{\xi\eta}[\mathbf{u}^{\xi}, \mathbf{u}^{\eta}]$ as the interatomic force acting on an atom whose type and position are indicated by ξ and $\mathbf{u}^{\xi}$, respectively, by an atom whose type and position are indicated by η and $\mathbf{u}^{\eta}$, respectively. The interatomic force in the Kth grain can now be expressed as

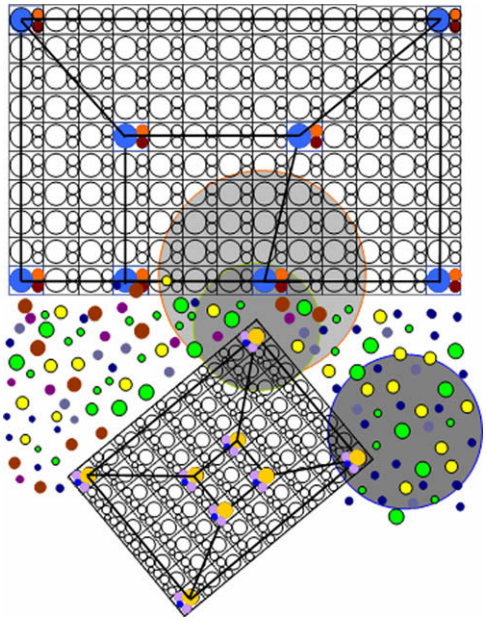

Fig. 2. Schematic diagram of multi-grain material system showing three representative *Cutoff* regions.

$$\begin{aligned}\mathbf{f}^{\alpha}(\mathbf{x},t;K) &= \sum_{j=1}^{N_a}\mathbf{f}^{\gamma(\alpha,K)\gamma(j)}\left[\mathbf{u}^{\alpha}(\mathbf{x},t;K),\mathbf{u}^{j}(t)\right] \\ &+ \sum_{L=1}^{N_g}\int_{\Omega_L(\mathbf{x}',t)}\frac{1}{V(\mathbf{x}',t;L)}\sum_{\beta=1}^{\upsilon(L)}\mathbf{f}^{\gamma(\alpha,K)\gamma(\beta,L)}\left[\mathbf{u}^{\alpha}(\mathbf{x},t;K),\mathbf{u}^{\beta}(\mathbf{x}',t;L)\right]d\Omega_L(\mathbf{x}',t)\end{aligned} \tag{24}$$

where Ω_L stands for the region of the *Lth* grain; $d\Omega_L$ is the differential volume in the *Lth* grain. The interatomic force in the atomic region can be expressed as

$$\begin{aligned}\mathbf{f}^{i}(t) = \sum_{j=1}^{N_a}\mathbf{f}^{\gamma(i)\gamma(j)}\left[\mathbf{u}^{i}(t),\mathbf{u}^{j}(t)\right] + \sum_{L=1}^{N_g}\int_{\Omega_L(\mathbf{x}',t)}\frac{1}{V(\mathbf{x}',t;L)} \\ \times\sum_{\beta=1}^{\upsilon(L)}\mathbf{f}^{\gamma(i)\gamma(\beta,L)}\left[\mathbf{u}^{i}(t),\mathbf{u}^{\beta}(\mathbf{x}',t;L)\right]d\Omega_L(\mathbf{x}',t)\end{aligned} \tag{25}$$

Henceforth, use the following notations

$$\begin{aligned}&\mathbf{u}^{i} = \mathbf{u}^{i}(t), \quad \mathbf{u}^{\alpha}(K) = \mathbf{u}^{\alpha}(\mathbf{x},t;K), \quad \mathbf{u}^{\beta}(\mathbf{x}';L) = \mathbf{u}^{\beta}(\mathbf{x}',t;L) \\ &\int_{\Omega_K}A\frac{d\Omega_K}{V} = \int_{\Omega_K(\mathbf{x},t)}A(\mathbf{x},t;K)\frac{d\Omega_K(\mathbf{x},t)}{V(\mathbf{x},t)} \\ &\int_{\Omega_L(\mathbf{x}')}A(\mathbf{x}')\frac{d\Omega_L(\mathbf{x}')}{V(\mathbf{x}')} = \int_{\Omega_L(\mathbf{x}',t)}A(\mathbf{x}',t;L)\frac{d\Omega_L(\mathbf{x}',t)}{V(\mathbf{x}',t)}\end{aligned} \tag{26}$$

Employ the pair potential for interatomic force

$$A \equiv \|\mathbf{A}\|, \quad \vec{\mathbf{A}} \equiv \mathbf{A}/A \tag{27}$$

In other words, $\mathbf{A}$ is any non-zero vector; A is the length of the vector; $\vec{\mathbf{A}}$ is a unit vector in the direction of $\mathbf{A}$. Therefore $\vec{\mathbf{A}}$ is parallel to $\mathbf{A}$ and $\mathbf{A} = A\vec{\mathbf{A}}$. Now the interatomic forces in Eqs. (24) and (25) can be expressed as

$$\begin{aligned}&\mathbf{f}^{\gamma(\alpha,K)\gamma(i)}\left[\mathbf{u}^{\alpha}(\mathbf{x},t;K),\mathbf{u}^{i}(t)\right] = f\left[r^{\gamma(\alpha,K)\gamma(i)},\gamma(\alpha,K),\gamma(i)\right]\vec{\mathbf{r}}^{\gamma(\alpha,K)\gamma(i)} \\ &\mathbf{r}^{\gamma(\alpha,K)\gamma(i)} \equiv \{\mathbf{x}+\mathbf{y}^{\alpha,K}+\mathbf{u}^{\alpha}(\mathbf{x},t;K)\} - \{\mathbf{x}^{i}+\mathbf{u}^{i}(t)\}\end{aligned} \tag{28}$$

$$\begin{aligned}&\mathbf{f}^{\gamma(\alpha,K)\gamma(\beta,L)}\left[\mathbf{u}^{\alpha}(\mathbf{x},t;K),\mathbf{u}^{\beta}(\mathbf{x}',t;L)\right] = f\left[r^{\gamma(\alpha,K)\gamma(\beta,L)},\gamma(\alpha,K),\gamma(\beta,L)\right]\vec{\mathbf{r}}^{\gamma(\alpha,K)\gamma(\beta,L)} \\ &\mathbf{r}^{\gamma(\alpha,K)\gamma(\beta,L)} = \{\mathbf{x}+\mathbf{y}^{\alpha,K}+\mathbf{u}^{\alpha}(\mathbf{x},t;K)\} - \{\mathbf{x}'+\mathbf{y}^{\beta,L}+\mathbf{u}^{\beta}(\mathbf{x}',t;L)\}\end{aligned} \tag{29}$$

$$\mathbf{f}^{\gamma(i)\gamma(j)}\left[\mathbf{u}^i(t),\mathbf{u}^j(t)\right]=f\left[r^{\gamma(i)\gamma(j)},\gamma(i),\gamma(j)\right]\vec{\mathbf{r}}^{\gamma(i)\gamma(j)}$$
$$\mathbf{r}^{\gamma(i)\gamma(j)}=\{\mathbf{x}^i+\mathbf{u}^i(t)\}-\{\mathbf{x}^j+\mathbf{u}^j(t)\} \tag{30}$$

$$\mathbf{f}^{\gamma(i)\gamma(\beta,L)}\left[\mathbf{u}^i(t),\mathbf{u}^\beta(\mathbf{x}',t;L)\right]=f\left[r^{\gamma(i)\gamma(\beta,L)},\gamma(i),\gamma(\beta,L)\right]\vec{\mathbf{r}}^{\gamma(i)\gamma(\beta,L)}$$
$$\mathbf{r}^{\gamma(i)\gamma(\beta,L)}=\{\mathbf{x}^i+\mathbf{u}^i(t)\}-\{\mathbf{x}'+\mathbf{y}^{\beta,L}+\mathbf{u}^\beta(\mathbf{x}',t;L)\} \tag{31}$$

For the pair potential, the interatomic force is parallel to the relative positions of the two atoms involved and the magnitude is a function of the types of the two atoms and the distance in between.

Now the weak form, based on Eqs. (22) and (23), it can be shown that

$$\sum_{K=1}^{N_g}\int_{\Omega_K}\sum_{\alpha=1}^{\upsilon(K)}\frac{1}{V}\{m^{\gamma(\alpha,K)}\ddot{\mathbf{u}}^\alpha(K)-\mathbf{f}^\alpha-\boldsymbol{\varphi}^\alpha\}\cdot\delta\mathbf{u}^\alpha(K)d\Omega_K+\sum_{i=1}^{N_a}\{m^{\gamma(i)}\ddot{\mathbf{u}}^i-\mathbf{f}^i-\boldsymbol{\varphi}^i\}\cdot\delta\mathbf{u}^i=0 \tag{32}$$

By using Eqs. (24) and (25), it can be further shown that

$$\begin{aligned}&\sum_{K=1}^{N_g}\sum_{\alpha=1}^{\upsilon(K)}\int_{\Omega_K}\Bigg\{m^{\gamma(\alpha,K)}\ddot{\mathbf{u}}^\alpha(K)\cdot\delta\mathbf{u}^\alpha(K)\\&-\sum_{L=1}^{N_g}\sum_{\beta=1}^{\upsilon(L)}\int_{\Omega_L(\mathbf{x}')}\mathbf{f}^{\gamma(\alpha,K)\gamma(\beta,L)}[\mathbf{u}^\alpha(K),\mathbf{u}^\beta(\mathbf{x}';L)]\cdot\delta\mathbf{u}^\alpha(K)\frac{d\Omega_L(\mathbf{x}')}{V(\mathbf{x}')}\\&-\sum_{i=1}^{N_a}\mathbf{f}^{\gamma(\alpha,K)\gamma(i)}[\mathbf{u}^\alpha(K),\mathbf{u}^i]\cdot\delta\mathbf{u}^\alpha(K)\\&-\sum_{i=1}^{N_a}\mathbf{f}^{\gamma(i)\gamma(\alpha,K)}[\mathbf{u}^i,\mathbf{u}^\alpha(K)]\cdot\delta\mathbf{u}^i-\boldsymbol{\varphi}^\alpha\cdot\delta\mathbf{u}^\alpha(K)\Bigg\}\frac{d\Omega_K}{V}\\&+\sum_{i=1}^{N_a}\left\{m^{\gamma(i)}\ddot{\mathbf{u}}^i-\sum_{j=1}^{N_a}\mathbf{f}^{\gamma(i)\gamma(j)}[\mathbf{u}^i,\mathbf{u}^j]-\boldsymbol{\varphi}^i\right\}\cdot\delta\mathbf{u}^i=0\end{aligned} \tag{33}$$

where $\delta\mathbf{u}^\alpha(K)\triangleq\delta\mathbf{u}^\alpha(\mathbf{x},t;K)$ is the virtual displacement at time t of the αth atom in the unit cell embedded at $\mathbf{x}$ which belongs to the Kth grain and $\delta\mathbf{u}^i$ is the virtual displacement of the ith atom in the atomic region. Suppose, for the Kth grain in the continuum region, the finite element mesh of the specimen has $N_p(K)$ nodes, $N_e(K)$ 8-node 3-D brick-type elements, each with eight Gauss points and the displacement field can be approximated as

$$\mathbf{u}^\alpha(\mathbf{x})=\sum_{\xi=1}^{8}\Phi_\xi(\mathbf{x})\mathbf{U}^{I_\xi(\mathbf{x})\alpha},\quad \delta\mathbf{u}^\alpha(\mathbf{x})=\sum_{\xi=1}^{8}\Phi_\xi(\mathbf{x})\delta\mathbf{U}^{I_\xi(\mathbf{x})\alpha} \tag{34}$$

where $\mathbf{U}^{I_\xi\alpha}$ and $\delta\mathbf{U}^{I_\xi\alpha}$ are the corresponding nodal values of $\mathbf{u}^\alpha$ and $\delta\mathbf{u}^\alpha$; $\boldsymbol{\Phi}_\xi(\mathbf{x})$ are the shape functions. It is also noticed that

$$\mathbf{f}^{\gamma(\alpha,K)\gamma(\beta,L)}\left[\mathbf{u}^\alpha(K),\mathbf{u}^\beta(\mathbf{x}';L)\right]=-\mathbf{f}^{\gamma(\beta,L)\gamma(\alpha,K)}\left[\mathbf{u}^\beta(\mathbf{x}';L),\mathbf{u}^\alpha(K)\right]$$
$$\mathbf{f}^{\gamma(\alpha,K)\gamma(i)}\left[\mathbf{u}^\alpha(K),\mathbf{u}^i\right]=-\mathbf{f}^{\gamma(i)\gamma(\alpha,K)}\left[\mathbf{u}^i,\mathbf{u}^\alpha(K)\right] \tag{35}$$

which will be utilized to ensure that the summation of interatomic force is vanishing. Then the weak form, Eq. (33), can be rewritten as

$$\begin{aligned}&\sum_{K=1}^{N_g}\sum_{\alpha=1}^{\upsilon(K)}\int_{\Omega_K}\Bigg\{\Phi_\xi\Phi_\eta\ddot{\mathbf{U}}^{I_\xi\alpha}\cdot\delta\mathbf{U}^{I_\eta\alpha}m^{\gamma(\alpha,K)}\\&-\frac{1}{2}\sum_{L=1}^{N_g}\sum_{\beta=1}^{\upsilon(L)}\int_{\Omega_L(\mathbf{x}')}\Phi_\eta(\mathbf{x})\delta\mathbf{U}^{I_\eta\alpha}\cdot\mathbf{f}^{\gamma(\alpha,K)\gamma(\beta,L)}\left[\mathbf{u}^\alpha(K),\mathbf{u}^\beta(\mathbf{x}';L)\right]\frac{d\Omega_L(\mathbf{x}')}{V(\mathbf{x}')}\\&+\frac{1}{2}\sum_{L=1}^{N_g}\sum_{\beta=1}^{\upsilon(L)}\int_{\Omega_L(\mathbf{x}')}\Phi_\eta(\mathbf{x}')\delta\mathbf{U}^{I_\eta(\mathbf{x}')\beta}\cdot\mathbf{f}^{\gamma(\alpha,K)\gamma(\beta,L)}\left[\mathbf{u}^\alpha(K),\mathbf{u}^\beta(\mathbf{x}';L)\right]\frac{d\Omega_L(\mathbf{x}')}{V(\mathbf{x}')}\\&-\sum_{i=1}^{N_a}\Phi_\eta(\mathbf{x})\delta\mathbf{U}^{I_\eta\alpha}\cdot\mathbf{f}^{\gamma(\alpha,K)\gamma(i)}\left[\mathbf{u}^\alpha(K),\mathbf{u}^i\right]-\Phi_\eta(\mathbf{x})\delta\mathbf{U}^{I_\eta\alpha}\cdot\boldsymbol{\varphi}^\alpha\Bigg\}\frac{d\Omega_K}{V}\\&+\sum_{i=1}^{N_a}\delta\mathbf{u}^i\cdot\left\{m^{\gamma(i)}\ddot{\mathbf{u}}^i-\sum_{j=1}^{N_a}\mathbf{f}^{\gamma(i)\gamma(j)}\left[\mathbf{u}^i,\mathbf{u}^j\right]-\sum_{i=1}^{N_a}\boldsymbol{\varphi}^i\right.\\&\left.+\sum_{K=1}^{N_g}\sum_{\alpha=1}^{\upsilon(K)}\int_{\Omega_K}\mathbf{f}^{\gamma(\alpha,K)\gamma(i)}\left[\mathbf{u}^\alpha(K),\mathbf{u}^i\right]\frac{d\Omega_K}{V}\right\}=0\end{aligned} \tag{36}$$

Denote

$$I_\eta\equiv IJK(K,I_e,\eta),\quad J_\eta\equiv IJK(\mathbf{x}',\eta) \tag{37}$$

where IJK stands for the connectivity of the finite element mesh. In other words, I_η is the node number of the ηth node of the I_eth element in the Kth grain, and J_η is the node number of the ηth node of the element in the Lth grain in which $\mathbf{x}'$ is located. In this work, we are using full order integration, i.e.,

$$\int_{\Omega_K}A(\mathbf{x})\frac{d\Omega_K}{V}=\sum_{I_e=1}^{N_e(K)}\sum_{g=1}^{8}A(I_e,g)\mathrm{N}(I_e,g) \tag{38}$$

where $N(I_e,g)\equiv J(I_e,g)/V(I_e,g)$ is the number of unit cells that the gth Gauss point of the I_eth element in the Kth grain represents and it is noticed that this number is constant in time. This is essentially the way to indicate that mass is conserved. Now, each integral term in Eq. (36) can be further derived to be

$$\begin{aligned}&\sum_{K=1}^{N_g}\sum_{\alpha=1}^{\upsilon(K)}\int_{\Omega_K}\Phi_\xi\Phi_\eta m^{\gamma(\alpha,K)}\frac{d\Omega_K}{V}\ddot{\mathbf{U}}^{I_\xi\alpha}\cdot\delta\mathbf{U}^{I_\eta\alpha}\\&\approx\sum_{K=1}^{N_g}\sum_{\alpha=1}^{\upsilon(K)}\sum_{I_e=1}^{N_e(K)}\sum_{g=1}^{8}\{\Phi_\xi(I_e,g)\Phi_\eta(I_e,g)\mathrm{N}(I_e,g)m^{\gamma(\alpha,K)}\}\ddot{\mathbf{U}}^{I_\xi\alpha}\cdot\delta\mathbf{U}^{I_\eta\alpha}\end{aligned} \tag{39}$$

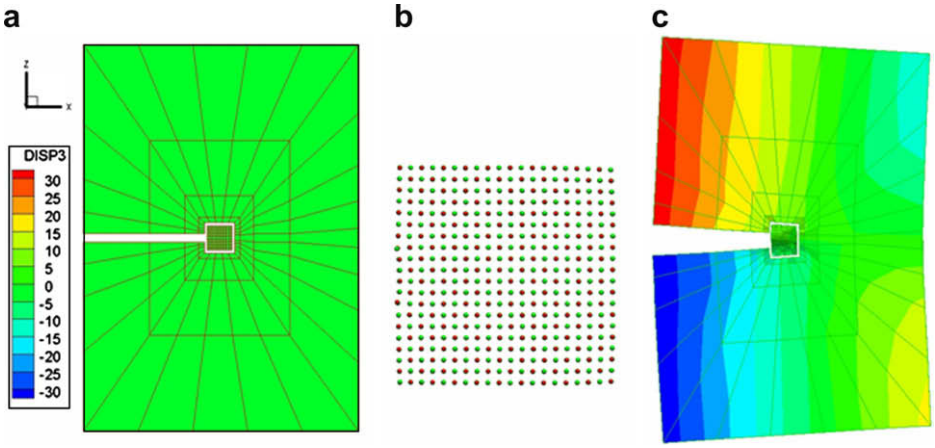

Fig. 3. The compact tension specimen: (a) finite element mesh with an atomic region (b) atoms in the atomic region (c) displacement (u_z) distribution on deformed shape.

$$\frac{1}{2}\sum_{K=1}^{N_g}\sum_{L=1}^{N_g}\sum_{\alpha=1}^{\upsilon(K)}\sum_{\beta=1}^{\upsilon(L)}\int_{\Omega_K}\int_{\Omega_L(\mathbf{x}')}\Phi_\eta(\mathbf{x})\mathbf{f}^{\gamma(\alpha,K)\gamma(\beta,L)}[\mathbf{u}^\alpha(\mathbf{x},K),\mathbf{u}^\beta(\mathbf{x}';L)]\times\frac{d\Omega_L(\mathbf{x}')}{V(\mathbf{x}')}\frac{d\Omega_K}{V}\cdot\delta\mathbf{U}^{I_\eta\alpha}$$
$$\approx\frac{1}{2}\sum_{K=1}^{N_g}\sum_{L=1}^{N_g}\sum_{\alpha=1}^{\upsilon(K)}\sum_{\beta=1}^{\upsilon(L)}\sum_{I_e=1}^{N_e(K)}\sum_{g=1}^{8}\Phi_\eta(I_e,g)\mathrm{N}(I_e,g)\delta\mathbf{U}^{I_\eta\alpha}\cdot\left\{\int_{\Omega_L(\mathbf{x}')}\mathbf{f}^{\gamma(\alpha,K)\gamma(\beta,L)}[\mathbf{u}^\alpha(I_e,g),\mathbf{u}^\beta(\mathbf{x}';L)]\frac{d\Omega_L(\mathbf{x}')}{V(\mathbf{x}')}\right\} \tag{40}$$

$$-\frac{1}{2}\sum_{K=1}^{N_g}\sum_{L=1}^{N_g}\sum_{\alpha=1}^{\upsilon(K)}\sum_{\beta=1}^{\upsilon(L)}\int_{\Omega_K}\int_{\Omega_L(\mathbf{x}')}\Phi_\eta(\mathbf{x}')\mathbf{f}^{\gamma(\alpha,K)\gamma(\beta,L)}[\mathbf{u}^\alpha(\mathbf{x};K),\mathbf{u}^\beta(\mathbf{x}';L)]\frac{d\Omega_L(\mathbf{x}')}{V(\mathbf{x}')}\times\frac{d\Omega_K}{V}\cdot\delta\mathbf{U}^{I_\eta(\mathbf{x}')\beta}$$
$$\approx-\frac{1}{2}\sum_{K=1}^{N_g}\sum_{L=1}^{N_g}\sum_{\alpha=1}^{\upsilon(K)}\sum_{\beta=1}^{\upsilon(L)}\sum_{I_e=1}^{N_e(K)}\sum_{g=1}^{8}\mathrm{N}(I_e,g)\times\left\{\int_{\Omega_L(\mathbf{x}')}\delta\mathbf{U}^{I_\eta\beta}\cdot\Phi_\eta(\mathbf{x}')\mathbf{f}^{\gamma(\alpha,K)\gamma(\beta,L)}[\mathbf{u}^\alpha(I_e,g),\mathbf{u}^\beta(\mathbf{x}';L)]\frac{d\Omega_L(\mathbf{x}')}{V(\mathbf{x}')}\right\} \tag{41}$$

$$\sum_{K=1}^{N_g}\sum_{\alpha=1}^{\upsilon(K)}\left\{\int_{\Omega_K}\Phi_\eta(\mathbf{x})\boldsymbol{\varphi}^\alpha(\mathbf{x})\frac{d\Omega_K}{V}\right\}\cdot\delta\mathbf{U}^{I_\eta\alpha}$$
$$\approx\sum_{K=1}^{N_g}\sum_{\alpha=1}^{\upsilon(K)}\sum_{I_e=1}^{N_e(K)}\sum_{g=1}^{8}\Phi_\eta(I_e,g)\mathrm{N}(I_e,g)\boldsymbol{\varphi}^\alpha(I_e,g)\cdot\delta\mathbf{U}^{I_\eta\alpha} \tag{42}$$

In the same pattern, one may like to make the following approximation

$$\sum_{K=1}^{N_g}\sum_{\alpha=1}^{\upsilon(K)}\sum_{i=1}^{N_a}\left\{\int_{\Omega_K}\Phi_\eta(\mathbf{x})\mathbf{f}^{\gamma(\alpha,K)\gamma(i)}\left[\mathbf{u}^\alpha(\mathbf{x};K),\mathbf{u}^i\right]\frac{d\Omega_K}{V}\right\}\cdot\delta\mathbf{U}^{I_\eta\alpha}$$
$$\approx\sum_{K=1}^{N_g}\sum_{\alpha=1}^{\upsilon(K)}\sum_{i=1}^{N_a}\sum_{I_e=1}^{N_e(K)}\times\sum_{g=1}^{8}\left\{\Phi_\eta(I_e,g)\mathrm{N}(I_e,g)\mathbf{f}^{\gamma(\alpha,K)\gamma(i)}\left[\mathbf{u}^\alpha(I_e,g),\mathbf{u}^i\right]\right\}\cdot\delta\mathbf{U}^{I_\eta\alpha} \tag{43}$$

However this term represents the atomistic interaction between the grains in the continuum region and the discrete atoms in the atomic region, we don't want to make such approximation and hence the interactions at the boundaries are fully counted. There is no need for any "transition zone" or any special treatment. The upgraded treatment is reflected later in Eqs. (44) and (45).

Because Eq. (36) has to be valid for any arbitrary virtual displacement $\delta\mathbf{U}^{I\beta}$ and $\delta\mathbf{u}^i$, where $I\in\{1,\sum_{K=1}^{N_g}N_p(K)\}$, $\beta\in\{1,\upsilon(K)\}$, $i\in\{1,N_a\}$, it leads to the following governing equations for nodal displacements and atomic displacements:

Continuum Region $K=1,2,3,\ldots,N_g$, $I=1,2,3,\ldots,\sum_{K=1}^{N_g}N_p(K)$, and $\beta=1,2,3,\ldots,\upsilon(K)$

$$\sum_{K=1}^{N_g}\sum_{I_e=1}^{N_e(K)}\sum_{g=1}^{8}\tilde{\delta}[I-I_\eta]m^{\gamma(\beta,K)}\Phi_\eta(I_e,g)\Phi_\xi(I_e,g)\mathrm{N}(I_e,g)\ddot{\mathbf{U}}^{I_\xi\beta}$$
$$-\frac{1}{2}\sum_{K=1}^{N_g}\sum_{I_e=1}^{N_e(K)}\sum_{g=1}^{8}\sum_{L=1}^{N_g}\sum_{\kappa=1}^{\upsilon(L)}\tilde{\delta}[I-I_\eta]\Phi_\eta(I_e,g)\mathrm{N}(I_e,g)\times\int_{\Omega_L(\mathbf{x}')}\mathbf{f}^{\gamma(\beta,K)\gamma(\kappa,L)}[\mathbf{u}^\beta(I_e,g),\mathbf{u}^\kappa(\mathbf{x}')]\frac{d\Omega_L(\mathbf{x}')}{V(\mathbf{x}')}$$
$$+\frac{1}{2}\sum_{K=1}^{N_g}\sum_{I_e=1}^{N_e(K)}\sum_{g=1}^{8}\sum_{L=1}^{N_g}\sum_{\kappa=1}^{\upsilon(K)}\tilde{\delta}[I-J_\eta]\mathrm{N}(I_e,g)\times\int_{\Omega_L(\mathbf{x}')}\Phi_\eta(\mathbf{x}')\mathbf{f}^{\gamma(\kappa,K)\gamma(\beta,L)}\left[\mathbf{u}^\kappa(I_e,g),\mathbf{u}^\beta(\mathbf{x}';L)\right]\frac{d\Omega_L(\mathbf{x}')}{V(\mathbf{x}')}$$
$$-\sum_{K=1}^{N_g}\sum_{i=1}^{N_a}\tilde{\delta}[I-I_\eta]\int_{\Omega_K}\Phi_\eta(\mathbf{x})\mathbf{f}^{\gamma(\beta,K)\gamma(i)}\left[\mathbf{u}^\beta(\mathbf{x};K),\mathbf{u}^i\right]\frac{d\Omega_K}{V}$$
$$-\sum_{K=1}^{N_g}\sum_{I_e=1}^{N_e(K)}\sum_{g=1}^{8}\tilde{\delta}[I-I_\eta]\mathrm{N}(I_e,g)\Phi_\eta(I_e,g)\boldsymbol{\varphi}^\beta=0 \tag{44}$$

Atomic region $i=1,2,3,\ldots,N_a$

$$m^{\gamma(i)}\ddot{\mathbf{u}}^i-\boldsymbol{\varphi}^i-\sum_{j=1}^{N_a}\mathbf{f}^{\gamma(i)\gamma(j)}[\mathbf{u}^i,\mathbf{u}^j]-\sum_{K=1}^{N_g}\sum_{\alpha=1}^{\upsilon(K)}\int_{\Omega_K}\mathbf{f}^{\gamma(i)\gamma(\alpha,K)}[\mathbf{u}^i,\mathbf{u}^\alpha(\mathbf{x})]\frac{d\Omega_K}{V}=0 \tag{45}$$

where $\tilde{\delta}$ is the Kronecker delta. It is emphasized that Eqs. (44) and (45) are the FE formulation of this multiscale field theory. Note that

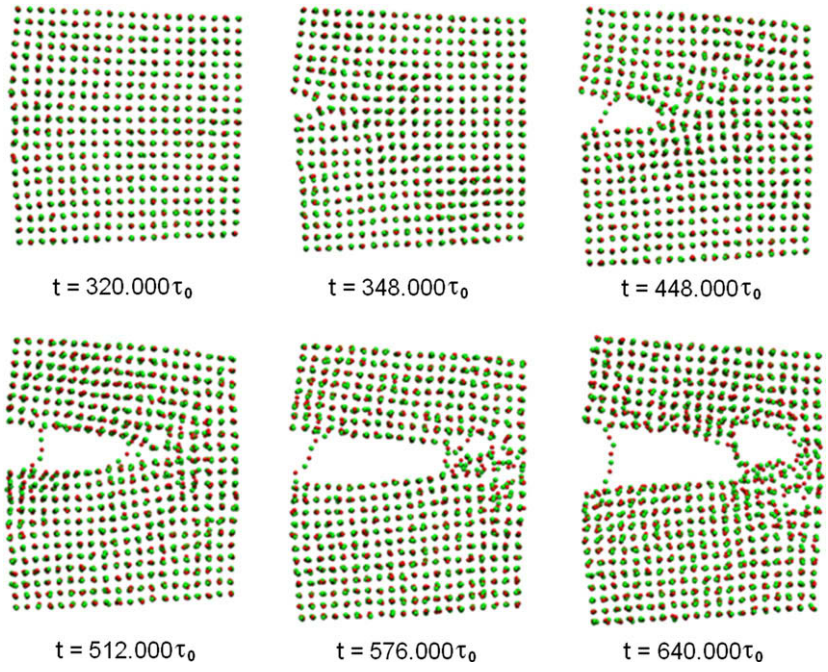

Fig. 4. Atomistic details of dynamic crack propagation.

involved in Eqs. (44) and (45) are the FE mesh with $\sum_{K=1}^{N_g} N_e(K)$ elements, the eight Gauss points per element, the shape functions $\Phi_\eta(I_e, g)$, the integration over $\Omega(\mathbf{x}')$, and the interatomic force $\mathbf{f}^{\gamma_1\gamma_2}$. It should also be emphasized that $\mathbf{f}^{\gamma_1\gamma_2}$ is calculated exactly the same way as in MD simulation.

It is noticed that the corresponding mass matrix $m^{\gamma(\beta,K)}\Phi_\eta(I_e, g)\Phi_\xi(I_e, g)\mathrm{N}(I_e, g)$ in Eq. (39) obtained from all Gauss points in all elements is symmetric but not diagonal. This is referred to as the distributed mass system. For the sake of dramatically reducing the computational effort, one would like to have a diagonal mass matrix, which is referred to as the lumped mass system. To do so, we let the eight Gauss points move toward their corresponding nodal points. In other words, let

$$\Phi_\xi(I_e, g) \to \delta_{\xi g} \tag{46}$$

By doing so, not only we end up with a lumped mass system, but also we convert the numerical implementation from Gauss integration to nodal integration if we choose to apply Eq. (46) to all other terms in Eqs. (44) and (45).

It is seen that Eqs. (44) and (45) are coupled sets of $3\sum_{K=1}^{N_g} \upsilon(K) N_p(K)$ and $3N_a$ second order ordinary differential equations, which can be readily solved by the central difference method. We have developed a computer software, named as MFT, which is based on the Multiscale Field Theory and the above-mentioned finite element formulation.

The idea of the finite element analysis of this multiscale theory can be further elaborated as follows. From Eq. (38), it is seen that we may further approximate the integral over the entire space $\Omega(\mathbf{x})$ by the Gauss quadrature

$$\int_{\Omega(\mathbf{x})} \mathbf{A}(\mathbf{x}) \frac{d\Omega(\mathbf{x})}{V(\mathbf{x})} \approx \sum_{I_e=1}^{N_e(K)} \sum_{g=1}^{8} \mathbf{A}(I_e, g)\mathrm{N}(I_e, g) \tag{47}$$

If one employs nodal integration in lieu of Gauss integration, then Eq. (47) can be rewritten as

$$\int_{\Omega(\mathbf{x})} \mathbf{A}(\mathbf{x}) \frac{d\Omega(\mathbf{x})}{V(\mathbf{x})} \approx \sum_{I_p=1}^{N_p} \mathbf{A}(I_p)\mathrm{N}(I_p) \tag{48}$$

where $\mathbf{A}(I_p)$ is the integrand evaluated at $I_p th$ node; N_p is the total number of FE nodes of the entire specimen; $N(I_p)$ is the weight of $I_p th$ node, which is equal to the number of unit cells that $I_p th$ node represents. It is worthwhile to note that all unit cells, hence all the atoms, in the specimen are represented by the FE nodes and each node is weighted according to the number of unit cells that it represents; all the nodes have interactions with all the atoms within their *Cutoff* regions. If one would like to have the whole specimen covered by overlapping *Cutoff* regions and also prefer to use large-size elements, one may use higher order Gauss integration of which the needed positions and weighting coefficients are given in [35].

4. Sample problem

We now present a sample problem to demonstrate the advantage and applicability of this multiscale field theory. Atomic units are used [28]. In this work, the material considered is *MgO*, a rock-salt-type crystal. Each unit cell has eight atoms: four Magnesium and four Oxygen. The Coulomb–Buckingham potentials between pairs of two atoms, *Mg–Mg*, *O–O*, *Mg–O*, are employed

$$V^{\xi\eta} = \frac{e^\xi e^\eta}{r^{\xi\eta}} + A^{\xi\eta} e^{-r^{\xi\eta}/B^{\xi\eta}} - C^{\xi\eta}/(r^{\xi\eta})^6 \tag{49}$$

where $A^{\xi\eta}$, $B^{\xi\eta}$, and $C^{\xi\eta}$ are material constants; $r^{\xi\eta} \equiv ||\mathbf{r}^{\xi\eta}|| \equiv ||\mathbf{r}^\xi - \mathbf{r}^\eta||$. The interatomic forces can be obtained as

$$\mathbf{f}(\xi;\eta) = -\frac{\partial V^{\xi\eta}}{\partial \mathbf{r}^\xi} = -\frac{\partial V^{\xi\eta}}{\partial r^{\xi\eta}} \frac{\mathbf{r}^{\xi\eta}}{r^{\xi\eta}} = \left\{ \frac{e^\xi e^\eta}{(r^{\xi\eta})^3} + \frac{A^{\xi\eta}}{B^{\xi\eta} r^{\xi\eta}} e^{-r^{\xi\eta}/B^{\xi\eta}} - 6\frac{C^{\xi\eta}}{(r^{\xi\eta})^8} \right\} \mathbf{r}^{\xi\eta}$$
$$\mathbf{f}(\eta;\xi) = -\frac{\partial V^{\xi\eta}}{\partial \mathbf{r}^\eta} = -\mathbf{f}(\xi;\eta) \tag{50}$$

The material constants used in this work are given in [28].

A compact tension specimen is shown in Fig. 3a. Discrete atoms are used in the crack-tip region as shown in Fig. 3a and Fig. 3b, while the material in the far field is modeled as a single crystal by the multiscale theory. The specimen occupies the space: $-50a \leqslant x \leqslant 50a$, $0 \leqslant y \leqslant 2a$, $-70a \leqslant z \leqslant 70a$. There are 42,756 unit cells (3,42,048 atoms) in the whole specimen, while 300 unit cells are in the crack-tip regions, modeled as 2400 distinct atoms. The lattice constant of *MgO* is a = 7.937 Bohr. The line crack extends from $x = -50a$ to $x = -6a$ at $z = 0$ through $y \in [0, 2a]$; and the separation of crack surfaces is $3a$. This means, in order to simulate the crack, two planes of atoms parallel to the crack surfaces are eliminated from the compact tension specimen. The FE mesh has 108 8-node elements and 280 nodes. The atomic region has 2400 discrete atoms. In this analysis, we use Δt = 40 τ_o, 16,000 number of time steps, and total time T_f = 6,40,000 τ_o = 15.47 pico seconds. The system is assumed to be initially at rest after a period of relaxation time and the boundary conditions are set as stress free except at

$$u_z^\alpha(-50a, y, z, t) = 5.25 \times 10^{-5} at/\tau_o \tag{51}$$

The displacement of a unit cell is defined as

$$\mathbf{u} \equiv \sum_{\alpha=1}^{8} \lambda^\alpha \mathbf{u}^\alpha \tag{52}$$

The displacement u_z at t = 6,40, 000 τ_o is displayed on deformed shape in Fig. 3c. The atoms in the crack-tip at various times are shown in Fig. 4, from which the process of dynamic crack propagation is clearly demonstrated. Our result shows that the crack propagates along the direction of the original line crack self-similarly, in other words, it propagates along the same crystallographic planes. This observation agrees with experimental studies in [36]. This is mainly because *MgO* is in the cubic phase and this specimen and the loading condition have a nearly perfect mirror symmetry with respect to the *y–z* plane. We also observe that the formation of secondary cracks in front of the primary crack. Similar phenomena in silicon have been reported in [37].

5. Conclusions

A multiscale field theory is introduced with the governing equations for multi-grain material system [21–25]. Although the multiscale theory is on the same physical foundation as MD simulation, we constructed a continuum theory, which is the field representation of atomistic *N – body* dynamics. Here, the term 'multi-grain material system' refers to a material system, which is made of more than one kind of grain and discrete atoms. Each grain is a 'multi-element system' which is made of more than one kind of chemical element. Therefore, in our multiscale theory, each point in the field represents one unit cell, which is made of several different and distinct atoms. For example, there are five atoms {one Bismuth, one Scadium, three Oxygen} in a unit cell of $BiScO_3$ and eight atoms {four Magnesium, four Oxygen} in a unit cell of *MgO*.

The balance law of linear momentum is used to formulate the dynamic equations of multi-grain material system. For each FE node in the *Kth* grain, there are $3\upsilon(K)$ displacements and $\upsilon(K)$ is the number of atoms in the unit cell, for example, υ = 5 for $BiScO_3$ and υ = 8 for *MgO*. It is noticed that υ = 1 only in classical continuum theory. Also, even at the continuum level, in the FE analysis,

the nodal forces are calculated through the use of interatomic potentials between different pairs of atoms. It is worthwhile to note that our formulation and analysis are dynamic, non-linear, and non-local. More importantly, in our computer software, the finest FE mesh one can use is equivalent to the crystal lattice, in other words, the smallest FE element size is equal to the lattice constant.

The irregular FE meshes are used for discrete atoms, for the study of dynamic crack propagation problem. It is natural to employ discrete atoms in the crack-tip region, large-sized elements in the far field, and small-sized elements between the two. It is noticed that from Fig. 3a, at the boundary between continuum region and atomic region, the FE mesh size does not need to match the lattice constant if one chooses not to. Also, there is no need for 'bridging' or 'transition' regions.

Acknowledgement

The authors acknowledge the support by National Science Foundation under Award Number CMMI-0646674.

References

[1] S.P. Xiao, T. Belytsckko, A bridging domain method for coupling continua with molecular dynamics, Comput. Methods Appl. Mech. Eng. 193 (2004) 1645.
[2] W.E.B. Engquist, X. Li, W. Ren, E. Vanden-Eijnden, The heterogeneous multiscale method: a review, Commun. Comput. Phys. 2 (3) (2007) 367.
[3] E.B. Tadmor, M. Ortiz, R. Phillips, Quasicontinuum analysis of defects in solids, Philo. Mag. 73 (1996) 1529.
[4] V.B. Shenoy, R.E. Miller, E.B. Tadmor, D. Rodney, R. Phillips, M. Ortiz, An adaptive methodology for atomic scale mechanics: the quasicontinuum method, J. Mech. Phys. Solids 47 (1998) 611.
[5] J. Knap, M. Ortiz, An analysis of the quasicontinuum method, J. Mech. Phys. Solids 49 (2001) 1899.
[6] B. Liu, Y. Huang, H. Jiang, S. Qu, K.C. Hwang, The atomic-scale finite element method, Comput. Methods Appl. Mech. Eng. 193 (2004) 1849.
[7] L.M. Dupuy, E.B. Tadmor, R.E. Miller, R. Phillips, Finite temperature quasicontinuum: molecular dynamics without all the atoms, Phys. Rev. Lett. 95 (2005) 060202.
[8] F.F. Abraham, J.Q. Broughton, N. Bernstein, E. Kaxiras, Spanning the continuum to quantum length scales in a dynamic simulation of brittle fracture, Europhys. Lett. 44 (6) (1998) 783.
[9] J.Q. Broughton, F.F. Abraham, N. Bernstein, E. Kaxiras, Concurrent coupling of length scales: methodology and applications, Phys. Rev. B 60 (1999) 2391.
[10] R.E. Rudd, J.Q. Broughton, Concurrent coupling of length scales in solid state systems, Phys. Status Solidi B 217 (2000) 251.
[11] R.E. Rudd, Concurrent multiscale modeling of embedded nanomechanics, Mater. Res. Soc. Symp. Proc. 677 (2001) AA1.6.1.
[12] E. Weinan, Z. Huang, Matching conditions in atomistic–continuum modeling of materials, Phys. Rev. Lett. 879 (2001) 135501.
[13] E. Weinan, Z. Huang, A dynamic atomistic–continuum method for the simulation of crystalline materials, J. Comput. Phys. 182 (2002) 234.
[14] X. Li, E. Weinan, Multiscale modeling of dynamics of solids at finite temperature, J. Mech. Phys. Solids 53 (2005) 1650.
[15] T. Belytsckko, S.P. Xiao, Coupling methods for continuum model with molecular model, J. Mult. Comput. Eng. 1 (2003) 115.
[16] S.P. Xiao, T. Belytsckko, A bridging domain method for coupling continua with molecular dynamics, Comput. Methods Appl. Mech. Eng. 193 (2004) 1645.
[17] G.J. Wagner, W.K. Liu, Coupling of atomistic and continuum simulations using a bridging scale decomposition, J. Comput. Phys. 190 (2003) 249.
[18] E.G. Karpov, G.J. Wagner, W.K. Liu, A Green's function approach to deriving non-reflecting boundary conditions in molecular dynamics simulations, Int. J. Numer. Methods Eng. 62 (9) (2005) 1250.
[19] A.C. To, S. Li, Perfectly matched multiscale simulations, Phys. Rev. B. 72 (3) (2005) 035414.
[20] W.A. Curtin, R.E. Miller, Atomistic/continuum coupling in computational materials science, Model. Simul. Mater. Sci. Eng. 11 (2003) R33.
[21] Y. Chen, Local stress and heat flux in atomistic systems involving three-body forces, J. Chem. Phys. 124 (2006) 054113.
[22] Y. Chen, J.D. Lee, Atomistic formulation of a multiscale theory for nano/micro physics, Philo. Mag. 85 (2005) 4095.
[23] Y. Chen, J.D. Lee, Conservation laws at nano/micro scales, J. Mech. Mater. Struct. 1 (2006) 681.
[24] Y. Chen, J.D. Lee, Y. Lei, L. Xiong, A multiscale field theory: nano/micro materials, in: G.C. Sih (Ed.), Multiscaling in Molecular and Continuum Mechanics, Springer, New York, 2006. 23.
[25] Y. Chen, J.D. Lee, L. Xiong, Stresses and strains at nano/micro scales, J. Mech. Mater. Struct. 1 (2006) 705.
[26] L. Xiong, Y. Chen, J.D. Lee, Atomistic measure of the strength of MgO nanorods, Theor. Appl. Fract. Mech. 46 (2006) 202.
[27] L. Xiong, Y. Chen, J.D. Lee, Atomistic simulation of mechanical properties of diamond and silicon by a field theory, Modelling Simul. Mater. Sci. Eng. 15 (2007) 35.
[28] J.D. Lee, Y. Chen, Modeling and simulation of a single crystal based on a multiscale field theory, Theor. Appl. Fract. Mech., submitted for publication.
[29] J.D. Lee, X. Wang, Y. Chen, Multiscale computation for nano/micro materials, ASCE J. Eng. Mech., submitted for publication.
[30] J.H. Irvine, J.G. Kirkwood, The statistical theory of transport processes. IV. The equations of hydrodynamics, J. Chem. Phys. 18 (1950) 817.
[31] R.J. Hardy, Formulas for determining local properties in molecular-dynamics simulations: shock waves, J. Chem. Phys. 76 (1) (1982) 622.
[32] K.S. Cheung, S. Yip, Atomic-level stress in an inhomogeneous system, J. Appl. Phys. 70 (10) (1991) 5688.
[33] J.M. Haile, Molecular Dynamics Simulation, Wiley, New York, 1992.
[34] M. Dove, Introduction to Lattice Dynamics, Cambridge University Press, Cambridge, 1993.
[35] O.C. Zienkiewicz, R.L. Taylor, The Finite Element Method, V.1 Basic Formulation and Linear Problems, McGraw-Hill, London, 1989.
[36] T. Crammer, A. Wanner, P. Gumbsch, Energy dissipation and path instabilities in dynamic fracture of silicon single crystals, Phys. Rev. Lett. 85 (2000) 788.
[37] M.J. Buehler, A.C.T. van Duin, W.A. Goddard III, Multiparadigm modeling of dynamical crack propagation in silicon using a reactive force field, Phys. Rev. Lett. 96 (9) (2006) 095505.